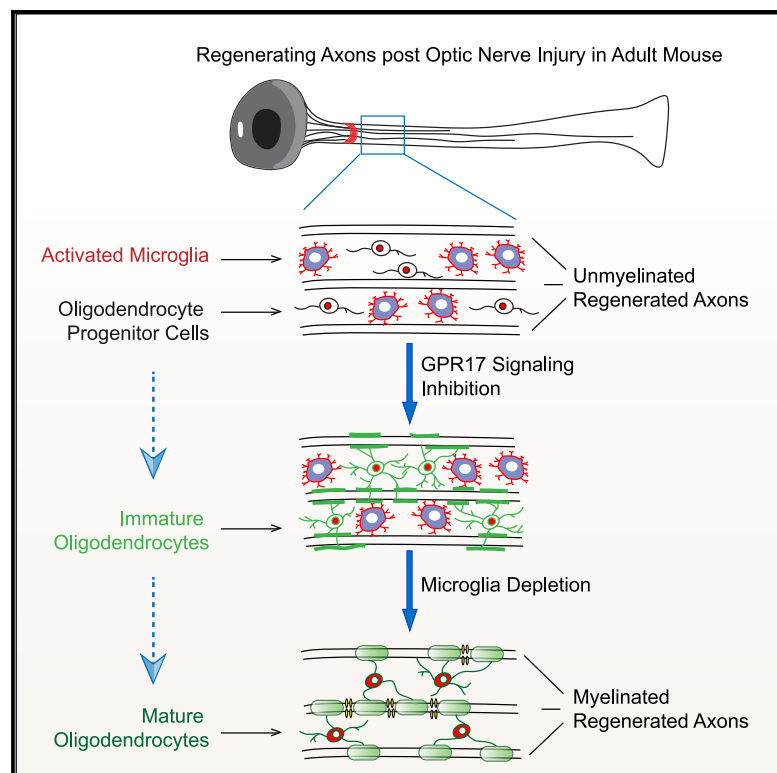


Robust Myelination of Regenerated Axons Induced by Combined Manipulations of GPR17 and Microglia

Graphical Abstract



Highlights

- Proliferated OPCs exhibit differentiation blockade in injured optic nerves
- GPR17 inhibition promotes OPC differentiation
- Chronically activated microglia prevent oligodendrocyte maturation
- Co-manipulation of GPR17 and microglia promotes robust myelination

Authors

Jing Wang, Xuelian He, Huyan Meng, ..., Jessica C. Page, Q. Richard Lu, Zhigang He

Correspondence

zhigang.he@childrens.harvard.edu

In Brief

While investigating why regenerated axons fail to be myelinated in injured optic nerves, Wang et al. find that injury-induced GPR17 expression in OPCs and chronically activated microglia suppress different steps of OPC differentiation. Co-manipulation of intrinsic (GPR17) and extrinsic (microglia) factors promotes extensive myelination of regenerated axons in an inflammatory environment.

Report

Robust Myelination of Regenerated Axons Induced by Combined Manipulations of GPR17 and Microglia

Jing Wang,^{1,3} Xuelian He,^{1,3} Huyan Meng,¹ Yi Li,¹ Phillip Dmitriev,¹ Feng Tian,¹ Jessica C. Page,¹ Q. Richard Lu,² and Zhigang He^{1,4,*}

¹F.M. Kirby Neurobiology Center, Boston Children's Hospital, and Department of Neurology and Ophthalmology, Harvard Medical School, Boston, MA, USA

²Department of Pediatrics, Brain Tumor Center, Division of Experimental Hematology and Cancer Biology, Cincinnati Children's Hospital Medical Center, Cincinnati, OH 45229, USA

³These authors contributed equally

⁴Lead Contact

*Correspondence: zhigang.he@childrens.harvard.edu

<https://doi.org/10.1016/j.neuron.2020.09.016>

SUMMARY

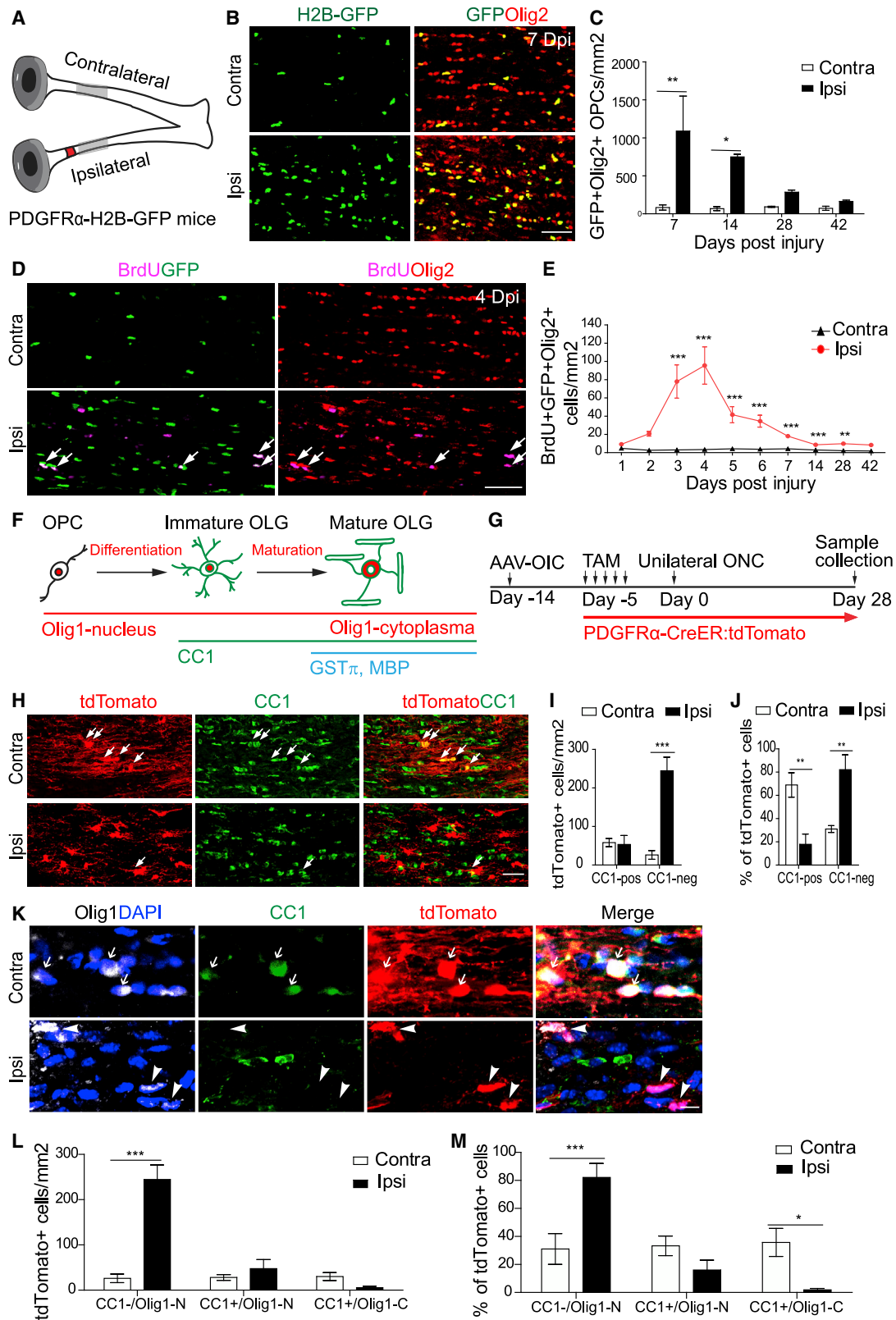
Myelination facilitates rapid axonal conduction, enabling efficient communication across different parts of the nervous system. Here we examined mechanisms controlling myelination after injury and during axon regeneration in the central nervous system (CNS). Previously, we discovered multiple molecular pathways and strategies that could promote robust axon regrowth after optic nerve injury. However, regenerated axons remain unmyelinated, and the underlying mechanisms are elusive. In this study, we found that, in injured optic nerves, oligodendrocyte precursor cells (OPCs) undergo transient proliferation but fail to differentiate into mature myelination-competent oligodendrocytes, reminiscent of what is observed in human progressive multiple sclerosis. Mechanistically, we showed that OPC-intrinsic GPR17 signaling and sustained activation of microglia inhibit different stages of OPC differentiation. Importantly, co-manipulation of GPR17 and microglia led to extensive myelination of regenerated axons. The regulatory mechanisms of stage-dependent OPC differentiation uncovered here suggest a translatable strategy for efficient *de novo* myelination after CNS injury.

INTRODUCTION

Functional deficits caused by CNS injury have been largely attributed to severing of long-projection axons. Despite tremendous progress toward developing strategies to promote axon regeneration, the behavioral and functional improvements achieved with these methodologies are still limited, even in experimental models (He and Jin, 2016; Hilton and Bradke, 2017; Benowitz et al., 2017). For example, our recent studies showed that the methods activating the mammalian target of rapamycin (mTOR) and STAT3 pathways in retinal ganglion cells (RGCs) promotes robust axon regeneration after optic nerve injury (Park et al., 2008; Duan et al., 2015) and that these regenerated axons can make functional synapses with their appropriate targets, such as the superior colliculus. However, regenerated RGC axons remain unmyelinated and ineffective at supporting visual functions (Bei et al., 2016). In light of the role of myelin in facilitating axon conduction, these observations point to a need to uncover the regulatory mechanisms of myelination after CNS injury.

For myelination in the adult CNS, residential oligodendrocyte precursor cells (OPCs) proliferate and then undergo a poorly

understood multi-step differentiation process before ultimately becoming myelination-competent oligodendrocytes (Simons and Nave, 2015; Chang et al., 2016; Monje, 2018). Demyelination and failure to re-myelinate underlie a number of neurological diseases, such as multiple sclerosis (MS) and Alzheimer's disease (Mathys et al., 2019). In the advanced stage of progressive MS, some proliferating OPCs remain in the lesions but fail to differentiate into mature oligodendrocytes (Wolswijk, 2002; Kuhlmann et al., 2008). Therefore, numerous efforts have been made to develop strategies that promote proliferation and differentiation of OPCs (Franklin and Ffrench-Constant, 2017). However, in most available demyelination models, remyelination occurs spontaneously, preventing precise examination of pro-myelination treatments that initiate *de novo* myelination. Furthermore, given the nature of the multi-step differentiation process required for transforming OPCs into mature oligodendrocytes, experimental perturbations targeting multiple steps may be required. In this regard, regenerated axons without spontaneous myelination in our optic nerve injury model serve as a "clean" model to assess the regulatory mechanisms of *de novo* myelination in the adult CNS. In this study, we wanted to find out how OPC proliferation and differentiation



(legend on next page)

occur in injured optic nerves and how barriers obstructing myelination of regenerated axons can be overcome. Our results revealed a set of translatable manipulations that enable robust myelination of regenerated axons in this model.

RESULTS

Injury-Induced OPC Proliferation

Our previous studies revealed that multiple different methods can elevate the intrinsic regenerative ability of RGCs and enable robust axon regeneration after injury. Intriguingly, these regenerated axons are not coupled with myelin-associated glycoprotein (MAG), implying that they are not myelinated (Bei et al., 2016). However, other studies have reported myelination of regenerated axons induced by different strategies (de Lima et al., 2012; Marin et al., 2016). Therefore, we assessed the myelination of regenerated axons induced by PTEN deletion in RGCs after an optic nerve crush injury. Among several thousands of axons analyzed, only two regenerated axons had thin myelin (Figures S1A and S1B). These results verified that most, if not all, regenerated optic nerve axons failed to undergo spontaneous myelination in our injury models.

Because OPCs are responsible for myelination in adults, we first assessed proliferation of OPCs in injured (ipsilateral) and control (contralateral) optic nerves of platelet-derived growth factor receptor α (PDGFR α)-H2B-GFP transgenic mice, in which all OPCs express nuclear H2B-GFP (Figure 1A). Because these mice also expressed GFP in less than 5% of vascular and leptomeningeal cells (Marques et al., 2016), we co-stained optic nerve sections with an oligodendrocyte lineage marker, Olig2, and defined the GFP+/Olig2+ double-positive cells as OPCs (Figures 1A–1C and S1C). As shown in Figures 1B, 1C, and S1C, the total numbers of OPCs in the crushed nerves increased significantly 1 and 2 weeks after injury but returned to the basal levels at 4 weeks. In contrast, low numbers of GFP+/Olig2+ OPCs were seen in intact nerves at all time points. To further assess injury-induced OPC proliferation, we administered bromodeoxyuridine (BrdU) at various time points after injury and evaluated BrdU incorporation 3 h post-injection with the expectation to label dividing OPCs at specific time points (Figures 1D and 1E). The results revealed that injury-induced OPC proliferation was increased significantly around 3–5 days after injury and subsequently reduced to basal levels at later time points (Figure 1E). Together, our results suggest that an optic nerve crush injury triggers rapid and reversible OPC proliferation.

Differentiation Failure of Proliferated OPCs in Injured Optic Nerves

To trace the differentiation of proliferated OPCs, we utilized a different reporter mouse line, PDGFR α -CreER (Young et al., 2013) crossed with Rosa26-STOP-tdTomato mice (Arenkiel et al., 2011) or PDGFR α -CreER:tdTomato mice. Upon tamoxifen administration, Cre expression is induced in PDGFR α + OPCs, resulting in tdTomato expression in OPCs and their progenies. The differentiation stages of these cells were assessed by immunohistochemistry with different markers: CC1 for all differentiated oligodendrocytes and Olig1, whose translocation from the nucleus to the cytoplasm is a hallmark for maturation into myelinating oligodendrocytes (Arnett et al., 2004; Gibson et al., 2019). Based on the results, lineage-traced cells could be divided into three stages: (1) undifferentiated OPCs (CC1– with nuclear Olig1), (2) immature oligodendrocytes (CC1+ with nuclear Olig1), and (3) mature oligodendrocytes (CC1+ with cytoplasmic Olig1) (Figure 1F). The identity of mature oligodendrocytes was also verified by additional markers of mature oligodendrocytes: GST π (Tansey and Cammer, 1991; Duncan et al., 2017) and myelin basic protein (MBP; Duncan et al., 2017; Figure 1F).

To promote axon regeneration, we injected AAVs expressing osteopontin/IGF1/CNTF (AAV-OIC) into the vitreous bodies of PDGFR α -CreER:tdTomato mice 2 weeks prior to optic nerve injury. To label pre-existing OPCs, tamoxifen was injected into these mice right before optic nerve crushing (Figure 1G). 4 weeks after injury, although the total tdTomato+ number is lower in intact optic nerves, 68% of tdTomato+ cells became CC1+ oligodendrocytes, and about half of them exhibited cytoplasmic Olig1+ (Figures 1H–1M). Noticeably, tdTomato+ cells had extensive processes in parallel with axons, indicating mature myelinating oligodendrocytes (Figure 1H). However, in injured optic nerves, only 18% tdTomato+ cells were CC1+ oligodendrocytes, and most had nuclear but not cytoplasmic Olig1 (Figures 1H–1M). Consistent with this, the majority of these tdTomato+ cells had short processes indicative of undifferentiated OPCs (Figure 1K). These results suggest that, in injured optic nerves, OPC differentiation is suppressed. Consistent with this, many GST π +tdTomato+ cells were seen in intact but not injured optic nerves (Figures S1D–S1F). In addition, although OPCs could differentiate into astrocytes during development (Levison and Goldman, 1993), we did not observe any tdTomato+ cells expressing the astrocyte marker GFAP (Figure S1G). Together, these data suggest that proliferated OPCs exhibit differentiation blockades in injured nerves,

Figure 1. Increased Proliferation and Failed Differentiation of OPCs in Injured Optic Nerves

(A) Scheme for the experiments shown in (A)–(C). The red spot indicates the crush injury site, and the gray region indicates the regions that were analyzed for this study.

(B and C) Images and quantification of OPC numbers in injured optic nerves at different time points after injury. $n = 3$ –8 mice per group.

(D and E) Images and quantification of BrdU+/Olig2+ cells in injured optic nerves.

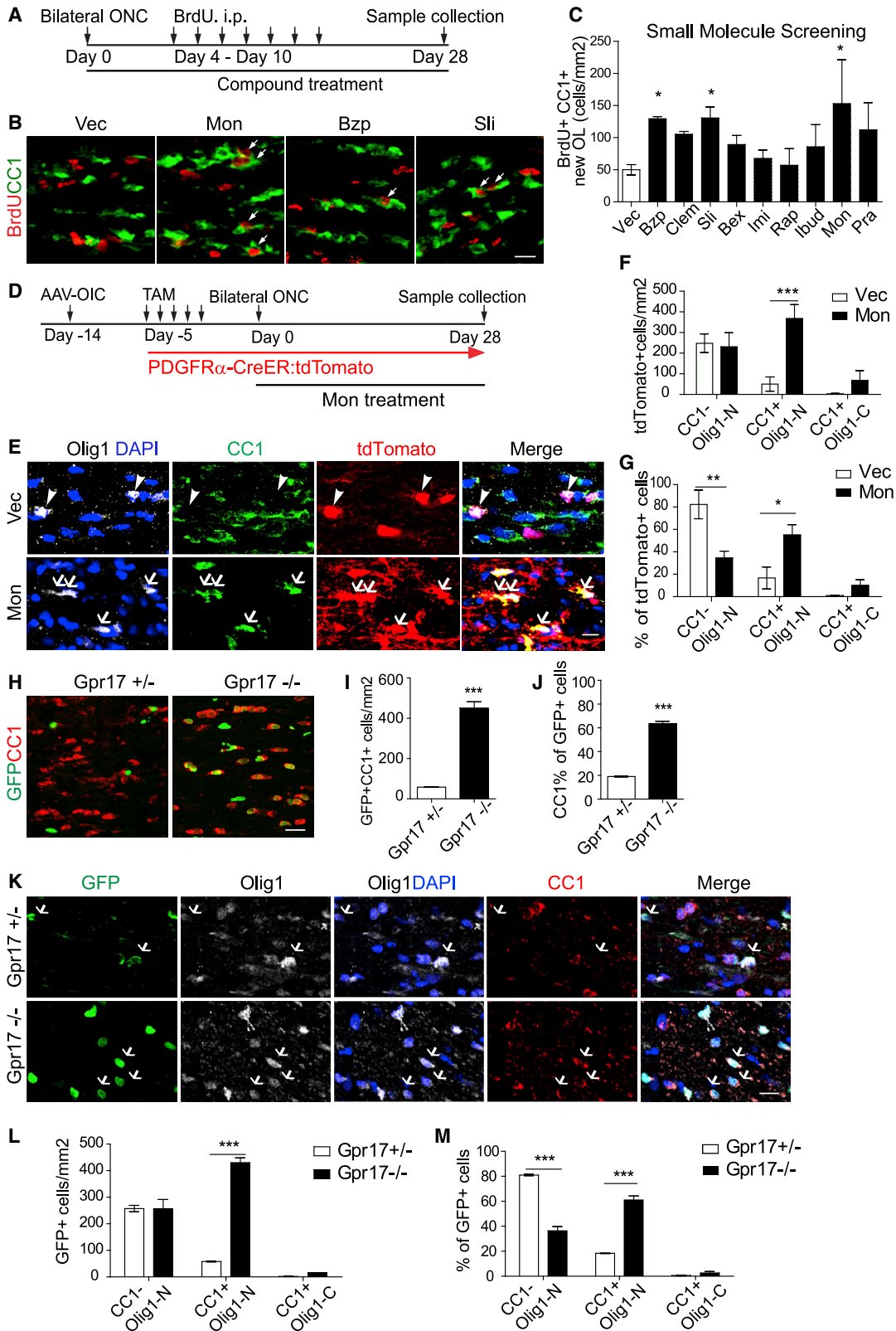
(F) Illustration of the differentiation stages of OPCs and their respective markers.

(G) Scheme for the experiments shown in (H)–(M). AAV-OIC: adeno-associated viruses (AAVs) expressing osteopontin/IGF1/CNTF1; TAM, tamoxifen; ONC, optic nerve crush.

(H–J) Images (H) and quantitation (cell number in I and proportion in J) of CC1+ and tdTomato+ cells. $n = 6$ mice per group.

(K–M) Images (K) and quantitation of three different populations. In (K), arrows on the contralateral side indicate tdTomato+/CC1+/Olig1–C, and arrowheads on the ipsilateral side indicate tdTomato+/CC1–/Olig1–N (undifferentiated cells). $n = 6$ mice per group.

Scale bars, 100 μ m (B and D), 50 μ m (H), and 10 μ m (K). * $p < 0.05$, ** $p < 0.01$, *** $p < 0.001$. Olig1–N, nuclear Olig1; Olig1–C, cytoplasmic Olig1. Data are presented as mean \pm SEM.



(legend on next page)

resembling what can be observed in the lesions of progressive MS patients.

Injury-Induced GPR17 Upregulation Contributes to the Early Differentiation Failure of OPCs

Previous studies with cultured cells and experimental autoimmune encephalomyelitis models identified a variety of compounds that could promote OPC proliferation and/or differentiation. However, it is unknown whether any of these agents could facilitate myelination of regenerated axons. To address this, we screened a set of small-molecule compounds with the goal to identify those that could increase OPC differentiation in injured optic nerves (Figures 2A–2C). Individual compound capable of penetrating the blood-brain barrier was administered systematically for 4 weeks after optic nerve injury in wild-type mice. To monitor the differentiation of proliferating OPCs, we applied daily BrdU injections from days 4–10 after injury, when OPCs exhibited a high proliferation rate (Figure 1E). The pro-differentiation effect of each compound was evaluated 4 weeks after administration (Figures 2A and 2B). As shown in Figures 2B and 2C, three compounds significantly increased the numbers of BrdU+/CC1+ double-positive cells: montelukast, a GPR17 antagonist (Fumagalli et al., 2011); benztropine mesylate, an M1/M3 muscarinic receptor antagonist (Deshmukh et al., 2013); and solifenacin, an M3 muscarinic receptor antagonist (Abiraman et al., 2015). Because montelukast had the strongest effect, our further studies focused on this compound and its putative target, GPR17.

As an initial verification, we applied montelukast treatment to PDGFR α -CreER/tdTomato mice after injury for 4 weeks (Figure 2D). As shown in Figures 2E–2G, 65% of tdTomato+ cells became CC1+, in contrast to 18% in vehicle-treated mice. Surprisingly, the majority of these CC1+/tdTomato+ cells had nuclear but not cytoplasmic Olig1 (Figures 2E–2G). In addition, the total tdTomato+ cell number increased after montelukast treatment (Figure 2F). Because cell death is associated with failed OPC differentiation (Hughes et al., 2018), such an increase in tdTomato+ cells may be secondary to the improved differentiation. Together, our results suggest that, although montelukast treatment promoted early differentiation of OPCs, these cells fail to advance into mature oligodendrocytes.

As an antagonist of leukotriene receptors, including GPR17 (Fumagalli et al., 2016), montelukast is a clinically approved treatment for asthma and seasonal allergies. GPR17 has been implicated previously as an inhibitor of oligodendrocyte differentiation (Chen et al., 2009; Simon et al., 2016; Ou et al., 2016).

However, GPR17 expression is downregulated in the adult CNS, and myelination appears to be normal in adult GPR17 knockout mice (Chen et al., 2009). By *in situ* hybridization, we found that GPR17 expression was rarely detectable in intact optic nerves of adult mice. However, optic nerve crush injury triggers significant upregulation of GPR17 in injured nerves (Figures S2A and S2B).

In addition to GPR17, montelukast may inhibit other leukotriene receptors (Leff et al., 1998). Thus, we assessed the effects of genetic deletion of GPR17 on OPC differentiation in injured optic nerves by utilizing GPR17 knockin mice (Chen et al., 2009). In this line, the GPR17 coding region is replaced with the H2B-GFP sequence. Thus, these mice could be used for monitoring GPR17 expression (by GFP signal in heterozygotes and homozygotes) and for loss-of-function studies (homozygotes). Consistent with injury-induced GPR17 expression, GFP+ (GPR17) cells were increased significantly in *GPR17*^{+/-} and *GPR17*^{-/-} mice 7 days after injury (Figures S2C–S2E). Most of these GFP+ cells were also co-stained with anti-Olig2, consistent with their restricted expression in the OPC lineage (Figure S2C). By 30 days after injury, many GFP+ cells were CC1+ in *GPR17*^{-/-} mice (Figures 2H–2J and S2F–S2H). However, these cells had nuclear but not cytoplasmic Olig1 signals (Figures 2L and 2M for day post injury [dpi] 28 and S2I–S2K for dpi 7), similar to montelukast treatment. In addition, the number of GFP+ cells was significantly higher in *GPR17*^{-/-} mice (Figures S2F–S2H). But these mice did not show increased proliferation by BrdU labeling (Figures S2C and S2E). Thus, increased GFP+ cells are likely secondary to improved differentiation. Similar to montelukast treatment, GPR17 knockout facilitated the initial differentiation, but not late maturation, of proliferated OPCs in injured optic nerves.

Differential Effects of Acutely or Sustained Activated Microglia on OPC Proliferation and Maturation

Because of the partial effects of GPR17 inhibition on OPC differentiation, we attempted to identify additional blocker(s) for the late maturation step of OPC differentiation. An important hint was the differing numbers of CC1+ cells with cytoplasmic Olig1 or GST π in injured versus control uninjured nerves (Figures 1K–1M and S1D–S1F), suggesting a possible contribution of environmental factors. Although similar levels of GFAP immunoreactivity were detected in injured and non-injured optic nerves (Figures S3A and S3B), microglia became rapidly and sustainably activated only in injured ones (Figures S3A–S3F). Because neuroinflammation has been shown to regulate OPC proliferation and differentiation (Franklin and Ffrench-Constant, 2017;

Figure 2. GPR17 Is an Intrinsic Blocker of Early Oligodendrocyte Differentiation of OPCs in Injured Optic Nerves

(A) Scheme of compound screening.

(B and C) Images of injured optic nerves stained with anti-CC1 and BrdU (B) and quantification (C). $n = 4$ –13 mice per group. Vec, vehicle; Mon, montelukast; Bzp, benztropine mesylate; Sli, solifenacin succinate.

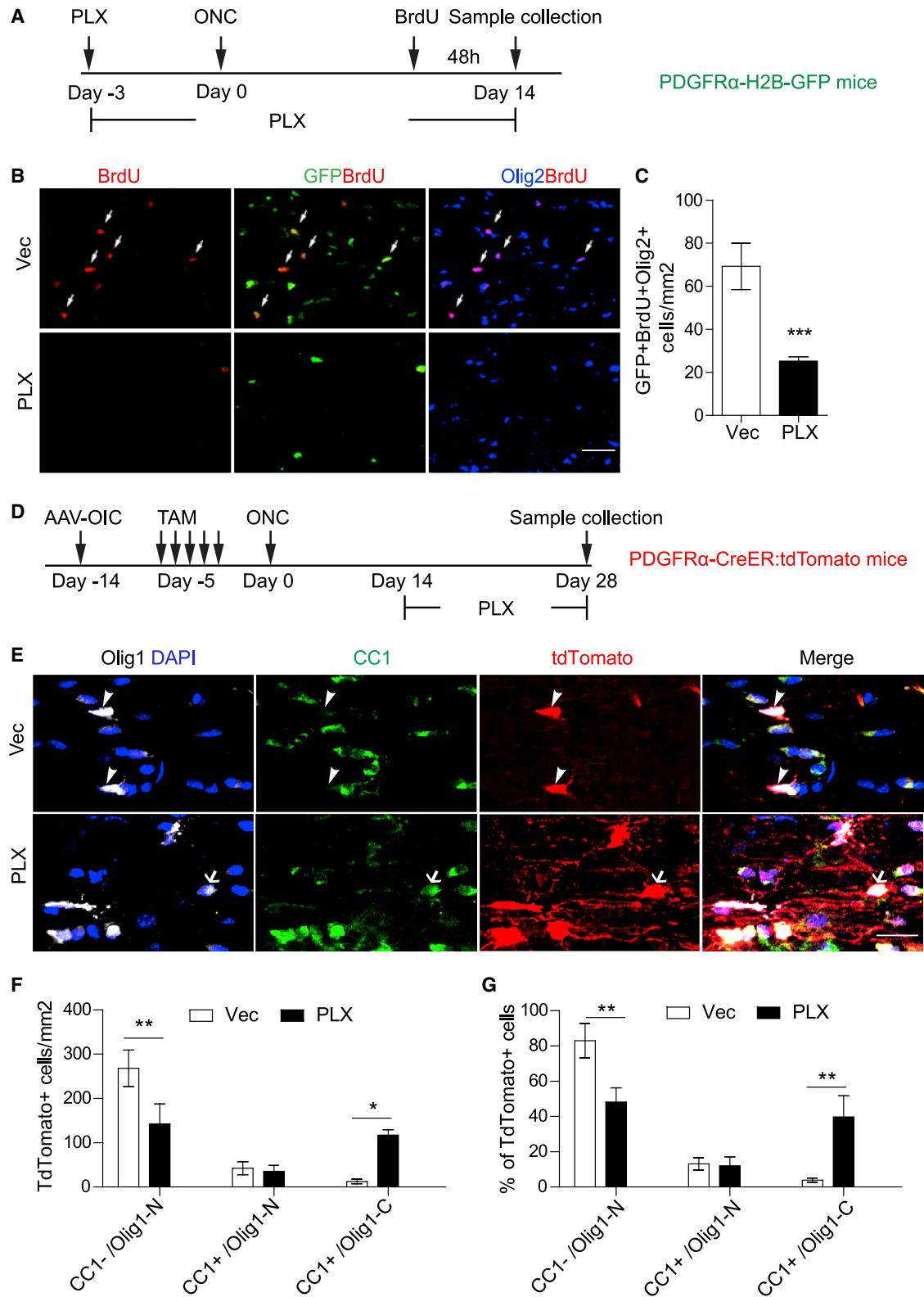
(D) Design for the experiments shown in (E)–(G). $n = 6$ mice per group.

(E–G) Images of injured or intact optic nerves stained with antibodies against Olig1, CC1, tdTomato, and DAPI (E) and quantification results of the densities (F) or proportions (G) of different populations. In (E), arrowheads indicate CC1⁻/Olig1⁻N cells in Vec, and arrows indicate CC1⁺/Olig1⁻N cells after treatment.

(H–J) Images of injured optic nerves 28 days after injury (H) and quantification results of the densities of GFP+/CC1+ cells (I) or proportion of CC1+ cells among GFP+ cells (J).

(K–M) Images (K) of injured optic nerves stained with the indicated antibodies and BrdU and quantification results of the densities (L) or proportions (M) of different populations. $n = 6$ mice per group.

Scale bars, 20 μ m (B and H), 10 μ m (E), and 20 μ m (K). * $p < 0.05$, ** $p < 0.01$, *** $p < 0.001$. Data are presented as mean \pm SEM.



(legend on next page)

Lassmann, 2018; Lloyd and Miron, 2019), we further examined the role of microglia in injured optic nerves on OPC proliferation and differentiation.

Taking advantage of the observation that systematic application of PLX3397, an inhibitor of colony-stimulating factor 1 receptor, depleted microglia *in vivo* (Figures S3J and S3K; Elmore et al., 2014), we first pre-treated PDGFR α -H2B-GFP mice with PLX3397 or control vehicle for 3 days before injury and continued the treatment for an additional 14 days before examining OPC proliferation by BrdU injection 48 h before euthanasia (Figure 3A). As shown in Figures 3B and 3C, PLX3397 profoundly reduced the total numbers of OPCs (BrdU+/GFP+/Olig2+). Thus, microglia activation is required for injury-induced OPC proliferation, consistent with early reports of a positive role of activated microglia in promoting myelination (Franklin and Ffrench-Constant, 2008; Miron et al., 2013; Lloyd and Miron, 2019).

Given that the majority of OPC proliferation occurs in the first week after injury (Figure 1E), we reasoned that delayed PLX3397 treatment 2–4 weeks after injury could bypass its inhibition on OPC proliferation, permitting us to assess its effects on OPC differentiation. Thus, PLX3397 was administered from 2–4 weeks after injury in PDGFR α -CreER:tdTomato mice, as used for Figures 1G–1M and 3D). This delayed PLX3397 treatment did not alter early differentiated OPCs (tdTomato+/CC1+/nuclear Olig1) but decreased the number of undifferentiated OPCs (tdTomato+/CC1–/nuclear Olig1) and, importantly, increased the number and proportion of mature oligodendrocytes (tdTomato+/CC1+/cytoplasmic Olig1) (Figures 3E–3G). Consistent with this, many of tdTomato+ cells had cytoplasmic Olig1 (Figures 3E–3G), were positive for GST π (Figure S4B), and exhibited elongated processes, likely undergoing myelination (Figure 3E).

To examine the activation states of microglia in injured optic nerves, we performed immunohistochemistry with antibodies against iNOS or arginase 1, markers for M1 and M2 microglia subtypes, respectively (Miron et al., 2013). As shown in Figures S3G–S3I, the numbers of Arg1+/Iba1+ cells were much lower than the overall number of iNOS+/Iba1+ cells. However, their expression patterns were similar at 7 dpi and 21 dpi, suggesting that other mechanisms, rather than M1/M2 dichotomy, account for the different activities of microglia in acute and chronic conditions (Marschallinger et al., 2020). Together, unlike for GPR17 inhibition (Figure 2), delayed ablation of microglia preferentially promoted maturation of early differentiated OPCs into myelinating oligodendrocytes.

Combination Treatment of Montelukast and PLX3397 Led to Robust Myelination of Regenerated Axons

Our observations concerning the differential effects of GPR17 inhibition and delayed microglia ablation on OPC differentiation

prompted us to assess the effects of combined treatments on myelination of regenerated axons. PDGFR α -CreER:tdTomato mice were treated with montelukast (for 4 weeks from dpi 1–28) and/or PLX3397 (for 2 weeks during dpi 15–28) after optic nerve crushing. As shown in Figures 4A–4C, the combined treatment dramatically increased the numbers of CC1+/tdTomato+ cells, and the majority of these CC1+ cells had cytoplasmic Olig1, implying that combination treatment promoted early and late differentiation of OPCs. Similar results were also obtained from immunohistochemistry with antibodies against GFT π and MBP (Figures S4A–S4F). Consistent with this, most of these tdTomato+ cells exhibited extensive elongating processes indicative of myelination (Figure 4A).

Subsets of mice in each treatment group were subjected to electron microscopy (EM) analysis (Figures 4D–4H) and additional immunohistochemistry (Figure 4I). As shown in Figures 4D and 4H, approximately 20% of regenerated axons were myelinated in mice treated with montelukast (15%) or PLX3397 (21%). However, after montelukast treatment, the myelin structures were noticeably thinner, consistent with our results showing that this compound promotes generation of early differentiated OPCs, which are only able to ensheath axons (Nave and Werner, 2014; Bercury and Macklin, 2015; Osso and Chan, 2017). In contrast, in mice with the combined treatment, the majority (60%) of regenerated axons were myelinated (Figures 4D and 4H). Many of these myelin structures were still thin and had large inner tongues, suggesting ongoing myelination (Figure 4E). Importantly, the nodes of Ranvier and sometimes semi-nodes could be detected by EM (Figures 4F and 4G) or immunohistochemistry (Figure 4I).

It is interesting that most of these regenerated axons have not crossed the optic chiasm, suggesting that induced myelination occurs before these regenerated axons form functional synapses with their functional targets. Additionally, we observed significantly more and longer regenerated axons with myelination-promoting treatments (Figures S4G–S4I), possibly related to protective effects of myelination on nascent axons (Simons and Nave, 2015; Morrison et al., 2013).

DISCUSSION

Our study established a combination treatment enabling robust myelination of regenerated axons in injured optic nerves. These results provide important insights, removing a major roadblock toward rebuilding functionally meaningful neuronal circuits (Laha et al., 2017; Williams et al., 2020). Importantly, the OPC dynamics observed in injured optic nerves have remarkable similarities with lesions in patients with progressive MS. Furthermore, persistently activated microglia dominate in injured optic

Figure 3. Microglia Are Required for OPC Proliferation but Detrimental for Their Maturation

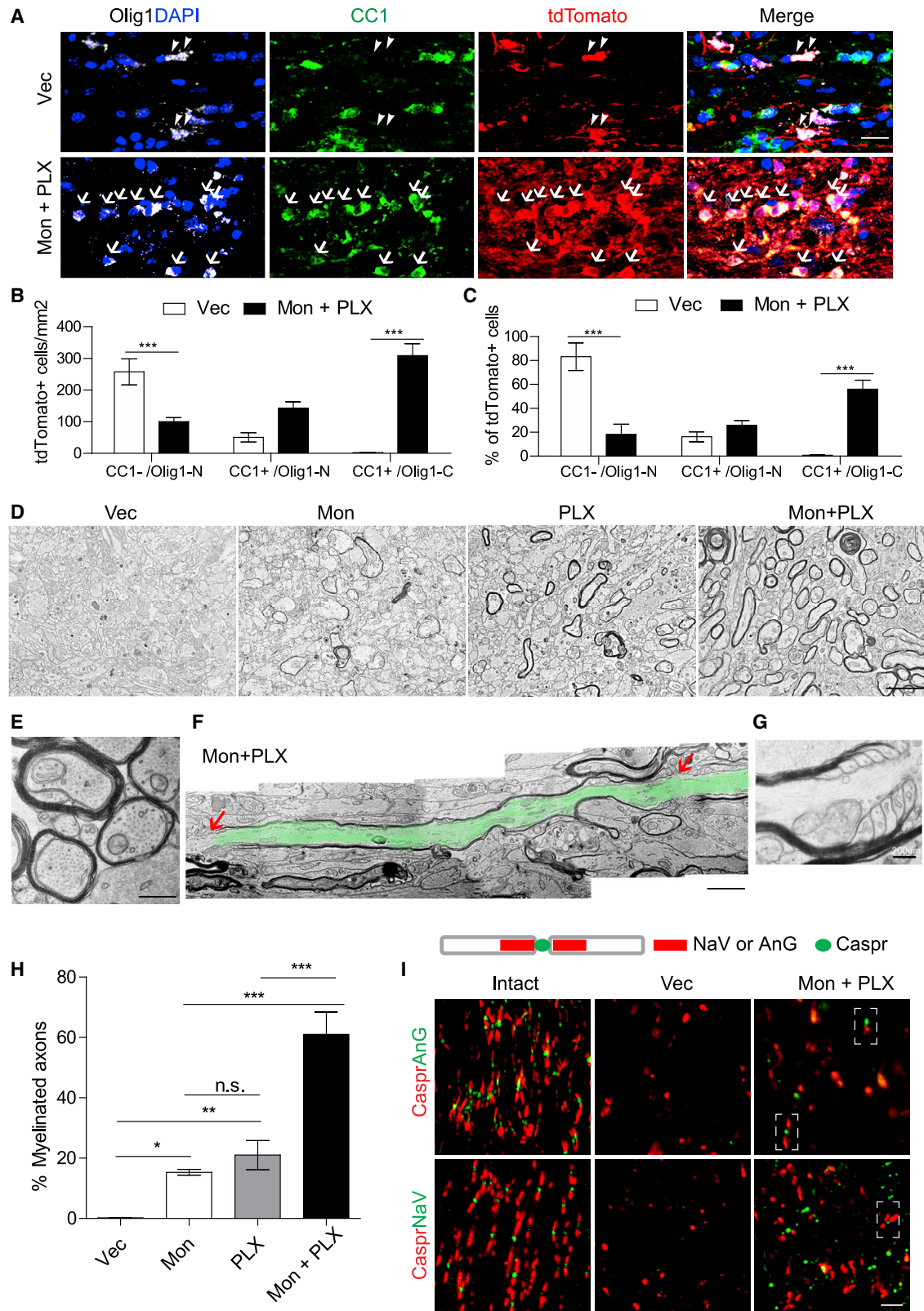
(A) Scheme for the experiments shown in (B) and (C).

(B and C) Images of injured optic nerves stained with GFP, Olig2, or BrdU (B) and quantification of the densities of GFP+/Olig2+/BrdU+ cells (C). n = 6 mice per group.

(D) Scheme for the experiments shown in (E)–(G).

(E–G) Images of injured optic nerves stained with the indicated antibodies or DAPI (E) and quantification results of the densities (F) or proportions (G) of different populations. In (E), arrowheads indicate CC1–/Olig1–N cells in Vec, and arrows indicate CC1+/Olig1–C cells after PLX treatment. n = 6 mice per group.

Scale bars, 100 μ m (B) and 25 μ m (E). *p < 0.05, **p < 0.01, ***p < 0.001. Data are presented as mean \pm SEM.



(legend on next page)

nerves (our results) and in MS lesions (Zrzavy et al., 2017). Thus, the results reported here could be informative for designing myelination-promoting interventions for progressive MS and other conditions.

Although montelukast could target GPR17 and other cysteinyl-leukotriene receptors (Hennen et al., 2013; Yokomizo et al., 2018), similar results observed in GPR17 knockout and montelukast-treated mice point toward GPR17 as a most relevant target. Interestingly, cells from the OPC lineage are increased significantly after GPR17 inhibition. Because this was not observed in knockout mice during development (Chen et al., 2009), this might be related to injury-associated factors. Indeed, GPR17 is known to be activated by cysteinyl-leukotrienes (Ciana et al., 2006). Thus, inflammation-elicited factors may activate GPR17, preventing GPR17-expressing OPCs from differentiation and even proliferating. These results highlight the importance of the interactions between environmental factors and OPC-intrinsic mechanisms in regulating their differentiation. In addition, other regulators may also play a role in this process because two M1/M3 muscarinic receptor antagonists also significantly increased OPC differentiation. Further studies will examine the effects of these molecules and their respective targets.

Our results also suggested a binary role of microglia in OPC dynamics. Although the majority of previous studies mainly emphasized a positive role of these activated microglia (Miron et al., 2013; Lloyd and Miron, 2019), Gibson et al. (2019) showed that chemotherapy-induced persistent activation of microglia contributes to impairment of OPC differentiation. Thus, our results may reconcile these prior findings. However, the molecular mechanisms underlying these different activities of microglia are still unclear. Furthermore, our results showed that co-manipulation of intrinsic (GPR17) and extrinsic (microglia) factors can achieve robust myelination of regenerated axons. Because myelination requires a sufficient number of mature oligodendrocytes differentiated from OPCs, our results highlight the need to target multiple steps and respective regulatory mechanisms for achieving robust (re)myelination. Future studies will examine whether such treatments enhance behavioral improvements in injury models and other pathological conditions.

STAR★METHODS

Detailed methods are provided in the online version of this paper and include the following:

- KEY RESOURCES TABLE
- RESOURCE AVAILABILITY
 - Lead Contact

- Materials Availability
- Data and code Availability
- EXPERIMENTAL MODEL AND SUBJECT DETAILS
 - Mouse Strains
 - Antibodies
- METHOD DETAILS
 - Virus Production
 - Surgical Procedures
 - AAV virus injections
 - Optic Nerve Injury
 - Compound Administration
 - Perfusions and Tissue Processing
 - Immunostaining and Imaging Analysis
 - Tissue Clearing, Imaging, and Quantification of Optic Nerve Regeneration
 - Electron Microscopy and Morphometric Analysis
 - *In situ* hybridization (FISH)
- QUANTIFICATION AND STATISTICAL ANALYSIS

SUPPLEMENTAL INFORMATION

Supplemental Information can be found online at <https://doi.org/10.1016/j.neuron.2020.09.016>.

ACKNOWLEDGMENTS

We thank J. Alberta and C. Stiles for providing anti-Olig1 antibodies, A. Effenberger for assistance, and Tracey Suter for critical reading of the manuscript. This study was supported by NIH grants R01EY021526 and R01EY026939 (to Z.H.) and grants from the Dr. Miriam and Sheldon G. Adelson Medical Research Foundation (to Z.H.). J.C.P. is supported by an F32 fellowship from NCCIH (F32AT011155). We thank the IDDRC and viral cores supported by NIH grants HD018655 and P30EY012196.

AUTHOR CONTRIBUTIONS

J.W., X.H., and Z.H. designed the experiments. J.W., X.H., Y.L., P.D., F.T., and J.C.P. performed the experiments and analyzed the data. Q.R.L. provided GPR17 mice. J.W., X.H., Y.L., J.C.P., and Z.H. wrote the paper with inputs from all authors.

DECLARATION OF INTERESTS

A patent based on the results in this manuscript was filed by Boston Children's Hospital (Z.H., J.W., and X.H. are co-inventors).

Received: May 18, 2020
Revised: August 13, 2020
Accepted: September 10, 2020
Published: October 26, 2020

Figure 4. Combination Treatment with Mon and PLX3397 Led to Robust Myelination of Regenerated Axons in Injured Optic Nerves

(A–C) Images of injured optic nerves stained with antibodies against Olig1, CC1, tdTomato, and DAPI (A) and quantification results of the densities (B) or proportions (C) of different populations. Arrowheads, CC1[−]/Olig1[−]N cells; arrows, CC1⁺/Olig1[−]C cells. n = 6 mice per group. (D–H) Transmission electron microscopic images (D–G) and quantification (H) of myelination of regenerated axons of injured optic nerves from mice with Mon and/or PLX3397 treatment. Low-magnification images of coronal sections (D) and quantification (H) of different groups. n = 4 for each group. An enlarged image (E) shows ongoing myelination, an image montage shows a complete internode highlighted in green (F), and also shown is an enlarged image of half of the nodes of Ranvier (G) from mice with combined treatment.

(I) Images of injured optic nerves with combined treatment stained with nodes of Ranvier markers.

Scale bars, 20 μ m (A), 2 μ m (D), 500 μ m (E), 1,400 nm (F), and 3.5 μ m (I). *p < 0.05, **p < 0.01, ***p < 0.001. Data are presented as mean \pm SEM.

REFERENCES

- Abiraman, K., Pol, S.U., O'Bara, M.A., Chen, G.D., Khaku, Z.M., Wang, J., Thorn, D., Vedia, B.H., Ekwegbalu, E.C., Li, J.X., et al. (2015). Anti-muscarinic adjunct therapy accelerates functional human oligodendrocyte repair. *J. Neurosci.* *35*, 3676–3688.
- Arenkiel, B.R., Hasegawa, H., Yi, J.J., Larsen, R.S., Wallace, M.L., Philpot, B.D., Wang, F., and Ehlers, M.D. (2011). Activity-induced remodeling of olfactory bulb microcircuits revealed by monosynaptic tracing. *PLoS ONE* *6*, e29423.
- Arnett, H.A., Fancy, S.P.J., Alberta, J.A., Zhao, C., Plant, S.R., Kaing, S., Raine, C.S., Rowitch, D.H., Franklin, R.J.M., and Stiles, C.D. (2004). bHLH transcription factor Olig1 is required to repair demyelinated lesions in the CNS. *Science* *306*, 2111–2115.
- Bei, F., Lee, H.H.C., Liu, X., Gunner, G., Jin, H., Ma, L., Wang, C., Hou, L., Hensch, T.K., Frank, E., et al. (2016). Restoration of Visual Function by Enhancing Conduction in Regenerated Axons. *Cell* *164*, 219–232.
- Benowitz, L.I., He, Z., and Goldberg, J.L. (2017). Reaching the brain: Advances in optic nerve regeneration. *Experimental Neurology* *287*, 365–373.
- Bercury, K.K., and Macklin, W.B. (2015). Dynamics and mechanisms of CNS myelination. *Dev. Cell* *32*, 447–458.
- Chang, K.J., Redmond, S.A., and Chan, J.R. (2016). Remodeling myelination: implications for mechanisms of neural plasticity. *Nat. Neurosci.* *19*, 190–197.
- Chen, Y., Wu, H., Wang, S., Koito, H., Li, J., Ye, F., Hoang, J., Escobar, S.S., Gow, A., Arnett, H.A., et al. (2009). The oligodendrocyte-specific G protein-coupled receptor GPR17 is a cell-intrinsic timer of myelination. *Nat. Neurosci.* *12*, 1398–1406.
- Choi, H.M.T., Schwarzkopf, M., Fornace, M.E., Acharya, A., Artavanis, G., Stegmaier, J., Cunha, A., and Pierce, N.A. (2018). Third-generation in situ hybridization chain reaction: Multiplexed, quantitative, sensitive, versatile, robust. *Development* *145*, dev165753.
- Ciana, P., Fumagalli, M., Trincavelli, M.L., Verderio, C., Rosa, P., Lecca, D., Ferrario, S., Parravicini, C., Capra, V., Gelosa, P., et al. (2006). The orphan receptor GPR17 identified as a new dual uracil nucleotides/cysteinyll-leukotrienes receptor. *EMBO J.* *25*, 4615–4627.
- de Lima, S., Koriyama, Y., Kurimoto, T., Oliveira, J.T., Yin, Y., Li, Y., Gilbert, H.Y., Fagiolini, M., Martinez, A.M., and Benowitz, L. (2012). Full-length axon regeneration in the adult mouse optic nerve and partial recovery of simple visual behaviors. *Proc. Natl. Acad. Sci. USA* *109*, 9149–9154.
- Deshmukh, V.A., Tardif, V., Lyssiotis, C.A., Green, C.C., Kerman, B., Kim, H.J., Padmanabhan, K., Swoboda, J.G., Ahmad, I., Kondo, T., et al. (2013). A regenerative approach to the treatment of multiple sclerosis. *Nature* *502*, 327–332.
- Duan, X., Qiao, M., Bei, F., Kim, I.J., He, Z., and Sanes, J.R. (2015). Subtype-specific regeneration of retinal ganglion cells following axotomy: effects of osetopontin and mTOR signaling. *Neuron* *85*, 1244–1256.
- Duncan, G.J., Plemel, J.R., Assinck, P., Manesh, S.B., Muir, F.G.W., Hirata, R., Berson, M., Liu, J., Wegner, M., Emery, B., et al. (2017). Myelin regulatory factor drives remyelination in multiple sclerosis. *Acta Neuropathol.* *134*, 403–422.
- Elmore, M.R.P., Najafi, A.R., Koike, M.A., Dagher, N.N., Spangenberg, E.E., Rice, R.A., Kitazawa, M., Matusow, B., Nguyen, H., West, B.L., and Green, K.N. (2014). Colony-stimulating factor 1 receptor signaling is necessary for microglia viability, unmasking a microglia progenitor cell in the adult brain. *Neuron* *82*, 380–397.
- Fox, R.J., Coffey, C.S., Conwit, R., Cudkovic, M.E., Gleason, T., Goodman, A., Klawiter, E.C., Matsuda, K., McGovern, M., Naismith, R.T., et al.; NN102/SPRINT-MS Trial Investigators (2018). Phase 2 trial of ibudilast in progressive multiple sclerosis. *N. Engl. J. Med.* *379*, 846–855.
- Franklin, R.J.M., and Ffrench-Constant, C. (2008). Remyelination in the CNS: from biology to therapy. *Nat. Rev. Neurosci.* *9*, 839–855.
- Franklin, R.J.M., and Ffrench-Constant, C. (2017). Regenerating CNS myelin - from mechanisms to experimental medicines. *Nat. Rev. Neurosci.* *18*, 753–769.
- Fumagalli, M., Daniele, S., Lecca, D., Lee, P.R., Parravicini, C., Fields, R.D., Rosa, P., Antonucci, F., Verderio, C., Trincavelli, M.L., et al. (2011). Phenotypic changes, signaling pathway, and functional correlates of GPR17-expressing neural precursor cells during oligodendrocyte differentiation. *J. Biol. Chem.* *286*, 10593–10604.
- Fumagalli, M., Lecca, D., and Abbracchio, M.P. (2016). CNS remyelination as a novel reparative approach to neurodegenerative diseases: The roles of purinergic signaling and the P2Y-like receptor GPR17. *Neuropharmacology* *104*, 82–93.
- Gibson, E.M., Nagaraja, S., Ocampo, A., Tam, L.T., Wood, L.S., Pallegar, P.N., Greene, J.J., Geraghty, A.C., Goldstein, A.K., Ni, L., et al. (2019). Methotrexate Chemotherapy Induces Persistent Tri-glial Dysregulation that Underlies Chemotherapy-Related Cognitive Impairment. *Cell* *176*, 43–55.e13.
- He, Z., and Jin, Y. (2016). Intrinsic Control of Axon Regeneration. *Neuron* *90*, 437–451.
- Hennen, S., Wang, H., Peters, L., Merten, N., Simon, K., Spinrath, A., Blättermann, S., Akkari, R., Schrage, R., Schröder, R., et al. (2013). Decoding signaling and function of the orphan G protein-coupled receptor GPR17 with a small-molecule agonist. *Sci. Signal.* *6*, ra93.
- Hilton, B.J., and Bradke, F. (2017). Can injured adult CNS axons regenerate by recapitulating development? *Development* *144*, 3417–3429.
- Hubler, Z., Allimuthu, D., Bederman, I., Elliott, M.S., Madhavan, M., Allan, K.C., Shick, H.E., Garrison, E., T Karl, M., Factor, D.C., et al. (2018). Accumulation of 8,9-unsaturated sterols drives oligodendrocyte formation and remyelination. *Nature* *560*, 372–376.
- Hughes, E.G., Orthmann-Murphy, J.L., Langseth, A.J., and Bergles, D.E. (2018). Myelin remodeling through experience-dependent oligodendrogenesis in the adult somatosensory cortex. *Nat. Neurosci.* *21*, 696–706.
- Kuhlmann, T., Miron, V., Cui, Q., Wegner, C., Antel, J., and Brück, W. (2008). Differentiation block of oligodendroglial progenitor cells as a cause for remyelination failure in chronic multiple sclerosis. *Brain* *131*, 1749–1758.
- Laha, B., Stafford, B.K., and Huberman, A.D. (2017). Regenerating optic pathways from the eye to the brain. *Science* *356*, 1031–1034.
- Lassmann, H. (2018). Multiple sclerosis pathology. *Cold Spring Harb. Perspect. Med.* *8*, a028936.
- Leff, J.A., Busse, W.W., Pearlman, D., Bronsky, E.A., Kemp, J., Hendeles, L., Dockhorn, R., Kundu, S., Zhang, J., Seidenberg, B.C., and Reiss, T.F. (1998). Montelukast, a leukotriene-receptor antagonist, for the treatment of mild asthma and exercise-induced bronchoconstriction. *N. Engl. J. Med.* *339*, 147–152.
- Levison, S.W., and Goldman, J.E. (1993). Both oligodendrocytes and astrocytes develop from progenitors in the subventricular zone of postnatal rat forebrain. *Neuron* *10*, 201–212.
- Lloyd, A.F., and Miron, V.E. (2019). The pro-remyelination properties of microglia in the central nervous system. *Nat. Rev. Neurol.* *15*, 447–458.
- Marin, M.A., de Lima, S., Gilbert, H.Y., Giger, R.J., Benowitz, L., and Rasband, M.N. (2016). Reassembly of Excitable Domains after CNS Axon Regeneration. *J. Neurosci.* *36*, 9148–9160.
- Marques, S., Zeisel, A., Codeluppi, S., Van Bruggen, D., Falcão, A.M., Xiao, L., Li, H., Häring, M., Hochgerner, H., Romanov, R.A., et al. (2016). Oligodendrocyte heterogeneity in the mouse juvenile and adult central nervous system. *Science* *352*, 1326–1329.
- Marschallinger, J., Schäffner, I., Klein, B., Gelfert, R., Rivera, F.J., Illes, S., Grassner, L., Janssen, M., Rotheneichner, P., Schmuckermair, C., et al. (2015). Structural and functional rejuvenation of the aged brain by an approved anti-asthmatic drug. *Nat. Commun.* *6*, 8466.
- Marschallinger, J., Iram, T., Zardeneta, M., Lee, S.E., Lehallier, B., Haney, M.S., Pluvinage, J.V., Mathur, V., Hahn, O., Morgens, D.W., et al. (2020). Lipid-droplet-accumulating microglia represent a dysfunctional and proinflammatory state in the aging brain. *Nat. Neurosci.* *23*, 194–208.
- Mathys, H., Davila-Velderrain, J., Peng, Z., Gao, F., Mohammadi, S., Young, J.Z., Menon, M., He, L., Abdurrob, F., Jiang, X., et al. (2019). Single-cell transcriptomic analysis of Alzheimer's disease. *Nature* *570*, 332–337.

- Mei, F., Fancy, S.P.J., Shen, Y.A.A., Niu, J., Zhao, C., Presley, B., Miao, E., Lee, S., Mayoral, S.R., Redmond, S.A., et al. (2014). Micropillar arrays as a high-throughput screening platform for therapeutics in multiple sclerosis. *Nat. Med.* **20**, 954–960.
- Meikle, L., Pollizzi, K., Egnor, A., Kramvis, I., Lane, H., Sahin, M., and Kwiatkowski, D.J. (2008). Response of a neuronal model of tuberous sclerosis to mammalian target of rapamycin (mTOR) inhibitors: effects on mTORC1 and Akt signaling lead to improved survival and function. *J. Neurosci.* **28**, 5422–5432.
- Miron, V.E., Boyd, A., Zhao, J.W., Yuen, T.J., Ruckh, J.M., Shadrach, J.L., van Wijngaarden, P., Wagers, A.J., Williams, A., Franklin, R.J.M., and Ffrench-Constant, C. (2013). M2 microglia and macrophages drive oligodendrocyte differentiation during CNS remyelination. *Nat. Neurosci.* **16**, 1211–1218.
- Monje, M. (2018). Myelin Plasticity and Nervous System Function. *Annu. Rev. Neurosci.* **41**, 61–76.
- Morrison, B.M., Lee, Y., and Rothstein, J.D. (2013). Oligodendroglia: metabolic supporters of axons. *Trends Cell Biol.* **23**, 644–651.
- Natrajan, M.S., de la Fuente, A.G., Crawford, A.H., Linehan, E., Nuñez, V., Johnson, K.R., Wu, T., Fitzgerald, D.C., Ricote, M., Bielekova, B., and Franklin, R.J. (2015). Retinoid X receptor activation reverses age-related deficiencies in myelin debris phagocytosis and remyelination. *Brain* **138**, 3581–3597.
- Nave, K.-A., and Werner, H.B. (2014). Myelination of the nervous system: mechanisms and functions. *Annu. Rev. Cell Dev. Biol.* **30**, 503–533.
- Ossio, L.A., and Chan, J.R. (2017). Architecting the myelin landscape. *Curr. Opin. Neurobiol.* **47**, 1–7.
- Ou, Z., Sun, Y., Lin, L., You, N., Liu, X., Li, H., Ma, Y., Cao, L., Han, Y., Liu, M., et al. (2016). Olig2-targeted G-protein-coupled receptor Gpr17 regulates oligodendrocyte survival in response to lysolecithin-induced demyelination. *J. Neurosci.* **36**, 10560–10573.
- Park, K.K., Liu, K., Hu, Y., Smith, P.D., Wang, C., Cai, B., Xu, B., Connolly, L., Kramvis, I., Sahin, M., et al. (2008). Promoting axon regeneration in the adult CNS by modulation of the PTEN/mTOR pathway. *Science* **322**, 963–966.
- Renier, N., Wu, Z., Simon, D.J., Yang, J., Ariel, P., and Tessier-Lavigne, M. (2014). IDISCO: A simple, rapid method to immunolabel large tissue samples for volume imaging. *Cell* **159**, 896–910.
- Simon, K., Hennen, S., Merten, N., Blättermann, S., Gillard, M., Kostenis, E., and Gomeza, J. (2016). The Orphan G Protein-coupled Receptor GPR17 Negatively Regulates Oligodendrocyte Differentiation via *Gαi/o* and Its Downstream Effector Molecules. *J. Biol. Chem.* **291**, 705–718.
- Simons, M., and Nave, K.A. (2015). Oligodendrocytes: Myelination and Axonal Support. *Cold Spring Harb. Perspect. Biol.* **8**, a020479.
- Tansey, F.A., and Cammer, W. (1991). A pi form of glutathione-S-transferase is a myelin- and oligodendrocyte-associated enzyme in mouse brain. *J. Neurochem.* **57**, 95–102.
- Williams, P.R., Benowitz, L.I., Goldberg, J.L., and He, Z. (2020). Axon Regeneration in the Mammalian Optic Nerve. *Annu. Rev. Vis. Sci.* **6**, 195–213.
- Wolswijk, G. (2002). Oligodendrocyte precursor cells in the demyelinated multiple sclerosis spinal cord. *Brain* **125**, 338–349.
- Yokomizo, T., Nakamura, M., and Shimizu, T. (2018). Leukotriene receptors as potential therapeutic targets. *J. Clin. Invest.* **128**, 2691–2701.
- Young, K.M., Psachoulia, K., Tripathi, R.B., Dunn, S.J., Cossell, L., Attwell, D., Tohyama, K., and Richardson, W.D. (2013). Oligodendrocyte dynamics in the healthy adult CNS: evidence for myelin remodeling. *Neuron* **77**, 873–885.
- Zrzavy, T., Hametner, S., Wimmer, I., Butovsky, O., Weiner, H.L., and Lassmann, H. (2017). Loss of ‘homeostatic’ microglia and patterns of their activation in active multiple sclerosis. *Brain* **140**, 1900–1913.

STAR★METHODS

KEY RESOURCES TABLE

REAGENT or RESOURCE	SOURCE	IDENTIFIER
Antibodies		
Rabbit anti-Olig1	Dr. Charles D Stiles	
Rabbit anti-Olig2	Novus biologicals	NBP1-28667
Rat anti-PDGFR α (CD140a)	BD Bioscience	558774
Mouse anti-CC1(APC)	Millipore	OP80
Rat anti-BrdU	Abcam	ab6326
Mouse anti-Nav1.6	Antibodies incorporated	75-026
Mouse anti-Ankyrin-G (AnkG)	Antibodies incorporated	75-146
Rabbit anti-Caspr	Abcam	ab34151
Rat anti-MBP	Abcam	ab7349
Mouse anti-MAG	Millipore	MAB1567
Rat anti-CD68	Bio-Rad	MCA1957
Rabbit anti-Iba1	WAKO Pure Chemicals	019-19741
Rabbit anti-P2Y12	AnaSpec	AS-55043A
Rat anti-GFAP	Thermo Fisher	13-0300
Mouse anti-GST- π	BD Transduction Laboratories	610718
Mouse anti-iNOS	BD Transduction Laboratories	610329
Mouse anti-Arginase 1	Santa Cruz Biotechnology	Sc-166920
Rabbit anti-RFP	Abcam	ab34771
<i>In situ</i> hybridization reagents		
HCR v3.0 kits	Molecular Instruments	
Chemicals, Peptides, and Recombinant Proteins		
Alexa-conjugated cholera toxin subunit B	Thermo Fisher	C34776
Fluoromont-G with DAPI	SouthernBiotech	0100-20
Tamoxifen	VWR	IC15673883
Bromodeoxyuridine (BrdU)	Sigma	B5002-1G
Glutaraldehyde	Electron Microscopy Sciences	16210
Benzotropine mesylate	PharmaBlock	Cat#N/A
Bexarotene	PharmaBlock	Cat#N/A
Clemastine Fumarate	PharmaBlock	Cat#N/A
Ibudilast	Selleckchem	S4837
Imidazole	Sigma	I5513-5G
Montelukast	PharmaBlock	Cat#N/A
Pranlukast	PharmaBlock	Cat#N/A
Rapamycin	PharmaBlock	Cat#N/A
Solifenacin succinate	PharmaBlock	Cat#N/A
Pexidartinib (PLX-3397)	PharmaBlock	Cat#N/A
Experimental Models: Organisms/Strains		
Mouse: C57BL/6	The Jackson Laboratory	Stock No: 000664
Mouse: PDGFR α -CreER	The Jackson Laboratory	Stock No: 018280
Mouse: PDGFR α -H2B-GFP	The Jackson Laboratory	Stock No: 007669
Mouse: Rosa26-STOP-tdTomato mice	Fan Wang lab	Arenkiel et al., 2011
Mouse: PTEN f/f	The Jackson Laboratory	Stock No: 034621

(Continued on next page)

Continued

REAGENT or RESOURCE	SOURCE	IDENTIFIER
Recombinant DNA		
pAAV-CAG-Cre	BCH Viral Core	N/A
pAAV-CAG-IGF1	BCH Viral Core	N/A
pAAV-CAG-CNTF	BCH Viral Core	N/A
pAAV-CAG-OPN	BCH Viral Core	N/A
Software and Algorithms		
ImageJ	NIH	RRID: SCR_003070
Prism 7.0	GraphPad Software	RRID: SCR_002798
MATLAB	Mathworks	N/A
Others		
LSM 700 scanning confocal microscope	Zeiss	N/A
LSM 710 scanning confocal microscope	Zeiss	N/A
TEM microscope	JEOL 1200EX - 80kV	N/A

RESOURCE AVAILABILITY

Lead Contact

Further information will be addressed by the Lead Contact, Zhigang He (zhigang.he@childrens.harvard.edu).

Materials Availability

For further requests for reagents, please contact the Lead Contact, Zhigang He (zhigang.he@childrens.harvard.edu).

Data and code Availability

This study did not generate datasets or codes that are available at the current stage.

EXPERIMENTAL MODEL AND SUBJECT DETAILS

Mouse Strains

All experimental procedures were performed in compliance with animal protocols approved by the Institutional Animal Care and Use Committee at Boston Children's Hospital. GPR17 transgenic mice were from Dr. Richard Lu ([Chen et al., 2009](#)). Other mouse strains were obtained from The Jackson Laboratory ([Key Resources Table](#)). Experiments started when mice reached 6-8 weeks old. Both male and female mice were randomized and assigned to different treatment groups, prior to injury, and no other specific randomization was used for the animal studies. Quantifications were examined blindly.

Antibodies

Primary antibodies used were: Rabbit anti-Olig1 (1:50, a gift from Dr. Charles D Stiles), rabbit anti-Olig2 (1:300, Novus biologicals, NBP1-28667), rat anti PDGFR α (CD140a) (1:100, BD Bioscience, 558774), mouse anti-CC1(APC) (1:100, Millipore, OP80), rat anti-BrdU (1:300, Abcam, ab6326), mouse Anti-Nav1.6 (1:50, Antibodies Incorporated, 75-026), mouse anti-Ankyrin-G (AnkG) (1:50, Antibodies Incorporated, 75-146), rabbit anti-Caspr (1:1000, Abcam, ab34151), rat anti-MBP (1:300, Abcam, ab7349), mouse anti-MAG (1:100, Millipore, MAB1567), rat anti-CD68 (1:300, Bio-Rad, MCA1957), rabbit anti-Iba1 (1:500, WAKO Pure Chemicals, 019-19741), rabbit anti-P2Y12 (1:500, AnaSpec, AS-55043A), rat anti-GFAP (1:1000, Thermo Fisher, 13-0300), mouse anti-GST pi (1:100, BD Transduction Laboratories, 610718), mouse anti-iNOS (1:200, BD Transduction Laboratories, 610329), mouse anti-Arginase 1 (1:100, Santa Cruz Biotechnology, sc-166920), and rabbit anti-RFP (1:500, Abcam, ab34771). Secondary antibodies with conjugated fluorophores were from Invitrogen.

METHOD DETAILS

Virus Production

All AAV viral vectors were made by Boston Children's Hospital Viral Core. AAV serotype 2 were used in our study as follows: AAV2-Cre; AAV2-CNTF; AAV2-IGF1; AAV2-OPN. The titers of all viral preparations were at least 1.0×10^{13} GC/ml.

Surgical Procedures

For all surgical procedures, mice were anaesthetized with ketamine and xylazine and received buprenorphine as a postoperative analgesic.

AAV virus injections

As previously described, intravitreal AAV injection was performed two weeks before optic nerve crush injury to enable axon regeneration. Briefly, a pulled-glass micropipette was inserted near the peripheral retina, behind the ora serrata, and deliberately angled to avoid damage to the lens. 2 μ l of AAV2/2-CAG-Cre virus was injected in PTEN *ff* mice (Park et al., 2008). 2 μ l of combined AAV2/2-CAG-CNTF, AAV2/2-CAG-IGF and AAV2/2-CAG-OPN (1:1:1 mix) was injected for other mouse strains (Bei et al., 2016).

Optic Nerve Injury

As previously described, the optic nerve was exposed intraorbitally and crushed with fine forceps (Dumont #5 FST) for 2 s, approximately 1 mm behind the optic disc. Afterward, eye ointment was applied postoperatively to protect the cornea. Robust axon regeneration could be observed at 2 weeks post-crush by Alexa-conjugated cholera toxin subunit B labeling.

Compound Administration

For PDGFR α -CreER mice, Tamoxifen (100 mg/kg, oral gavage) was administered daily for 5 days immediately preceding optic nerve crush. For OPC proliferation assays, BrdU (100 mg/kg, intraperitoneal injection) was injected at either 3 hours or 48 hours before sample collection. For compound screening, BrdU was injected from day 4–10 post optic nerve crush. Each compound or the vehicle was administered daily for four weeks, starting from day 1 post optic nerve crush. Tested compounds include: Bzopropine mesylate (Bzp), a M1/M3 muscarinic receptor antagonist (Deshmukh et al., 2013; 10 mg/kg, i.p.), clemastine (Clem), an antihistamine and anticholinergic agent, M1/M3 muscarinic receptor antagonist (Mei et al., 2014; 10 mg/kg, p.o.), Solifenacin (Sli), a M3 muscarinic receptor antagonist (Abiraman et al., 2015; 20 mg/kg, i.p.), Bexarotene (Bex), a retinoid X receptor agonist (Natrajan et al., 2015; 100 mg/kg, p.o.), imidazole (Imi), an anti-cholesterol synthesis compound (Hubler et al., 2018; 10 mg/kg, i.p.), Ibudilast (Ibud), a clinically-approved phosphodiesterase (PDE) inhibitor (Fox et al., 2018; 10 mg/kg, i.p.), and Montelukast (Mon, 25 mg/kg, p.o.), and Pranlukast (Pra, 0.5 mg/kg, i.p.), two different GPR17 antagonists (Fumagalli et al., 2011; Marschallinger et al., 2015; Ou et al., 2016). Rapamycin (Rap, 6 mg/kg, i.p.), a mTOR inhibitor, was also included in our screening as it was shown to improve myelination in TSC1 knockout mice (Meikle et al., 2008). Pexidartinib (PLX 3397) was mixed in food chow at 290 mg/kg by LabDiet laboratory animal nutrition.

Perfusions and Tissue Processing

For immunostaining, mice were given an overdose of anesthesia and transcardiacally perfused with ice cold PBS followed by 4% paraformaldehyde (PFA, Sigma-Aldrich). After perfusion, optic nerves were dissected out and post-fixed in 4% PFA overnight at 4°C. Tissues were cryoprotected by sinking in 30% sucrose (in 1X phosphate buffered saline (PBS) for 48 hours. Samples were frozen in Optimal Cutting Temperature compound (Tissue Tek) using dry ice and then sectioned at 12 μ m for optic nerves.

Immunostaining and Imaging Analysis

Cryosections (12 μ m thick) were permeabilized, incubated in blocking buffer (0.5% Triton X-100 and 5% normal goat serum in PBS) for 1 h at room temperature, and overlaid with primary antibodies overnight at 4°C. For BrdU staining, cells or tissue sections were denatured with HCl (2N) for 30 minutes at 37°C and then neutralized with 0.1 M sodium borate buffer for 10 min before proceeding to the normal blocking procedure. On the next day, the corresponding Alexa Fluor 488-, 594- or 647-conjugated secondary antibodies were applied (all secondary antibodies were purchased from Invitrogen). All stained sections were mounted with DAPI-containing mounting solution and sealed with glass coverslips. All immunofluorescence-labeled images were acquired using a Zeiss 700 or Zeiss 710 confocal microscope. Images were taken within 1mm distal region from the crush site since this area contains the highest number of regenerated axons (shadow area in Figure 1A). For each biological sample, 3–5 sections of each optic nerve were imaged under 10x or 20x objectives for quantification. For whole nerve images, Tiles function was applied to stitch individual scanning image on Zeiss 710 (Figure S3E). Positive cell numbers were then quantified manually using the Plugins/ Analyze /Cell Counter function in ImageJ software. For fluorescent intensity analysis, the images were first converted to 8-bit depth in ImageJ software and then the mean intensity value was calculated by the build-in function: Analyze/Measure.

Tissue Clearing, Imaging, and Quantification of Optic Nerve Regeneration

Mice injected with fluorophore tagged Cholera Toxin B (CTB) were perfused with 4% paraformaldehyde. Dissected optic nerves were then subjected to a modified procedure from previously published iDISCO tissue clearing method (Renier et al., 2014). Briefly, optic nerve samples were incubated in the dark for 0.5 h of 80% tetrahydrofuran (THF, Sigma-Aldrich 360589-500ML)/H₂O and then switched to 100% THF for 1 hour for dehydration. Then, samples were incubated in Dichloromethane (DCM, Sigma-Aldrich 270997-1L) for 20 minutes. Samples were finally switched to dibenzyl ether (DBE, Sigma-Aldrich 33630-250ML) until completely transparent (at least 3 hours, but overnight is recommended). For imaging, processed nerves can be mounted in DBE and imaged under Zeiss 710 confocal microscope using Z stack and Tiles functions. Z stack scanning and maximum projection of images were used in order to capture all regenerated axons. For image analysis, fluorescent intensity profile along the nerve was generated by the

build-in function of ImageJ: Analyze/Plot Profile. To calculate the integral of fluorescent intensity across the entire length of the nerve, a custom MATLAB algorithm was developed by our lab to quantify the “area under curve” from the plot profile data generated by ImageJ.

Electron Microscopy and Morphometric Analysis

Mice were perfused with 4% paraformaldehyde containing 2.5% glutaraldehyde in 0.1 M sodium cacodylate buffer, pH 7.2. Optic nerves were dissected and placed in this fixative overnight. Samples were then processed by EM Core facility at Harvard Medical School, with the following procedure: samples were rinsed in PBS, post-fixed in 1% OsO₄ in PBS for 1 h, dehydrated in a graded ethanol series, infiltrated with propylene oxide, and embedded in Epon. Semithin sections were stained with toluidine blue, and ultrathin sections were stained with lead citrate. Ultrathin sections were taken under JEOL 1200EX – 80kV electron microscope. The number of myelinated axons per nerve was analyzed in ultrathin sections at magnifications 3,000x to 20,000x. To better distinguish new myelin from pre-existing myelin, areas with regenerated axons and no myelin debris were selected for quantification. For longitudinal images of Nodes of Ranvier (Figure 4F), individual images were stitched in photoshop software by automatic stitching.

In situ hybridization (FISH)

To assess the expression pattern of GPR17, we performed *in situ* hybridization by hybridization chain reaction (HCR) (Choi et al., 2018) with a commercial kit containing a DNA probe set, a DNA HCR amplifier, and different buffers (Molecular Instruments). To prepare sections, anesthetized mice were perfused with DEPC-PBS followed by 4% paraformaldehyde (PFA). Dissected optic nerves were fixed in 4% PFA overnight, dehydrated in 30% sucrose/DEPC-PBS at 4°C, embedded in OCT and cryosectioned at 14 μm. Tissues were permeabilized in 5% SDS for 20 min at room temperature (RT) and pre-hybridized in hybridization buffer for 3 hours at 37°C. Then slides were incubated in pre-warmed hybridization buffer including probes (2.5 nM for each) at 37°C overnight. After hybridization, slices were washed for 1 hour at 37°C with wash buffer followed by 2xSSC or 15 minutes at room temperature. The amplification step was performed with B3 HCR amplifiers for overnight.

QUANTIFICATION AND STATISTICAL ANALYSIS

Normality and variance similarity were measured by STATA before we applied any parametric tests. Two-tailed Student’s t test was used for single comparisons between two groups. Other data were analyzed using one-way or two-way ANOVA depending on the appropriate design. *Post hoc* comparisons were carried out only when the primary measure showed statistical significance. P value of multiple comparisons was adjusted using Bonferroni’s correction. Error bars in all figures represent mean ± SEM. Mice with different litters, body weights, and sexes were randomized and assigned to different treatment groups, and no other specific randomization was used for the animal studies.